



3D characterization of the subsurface redox architecture in complex geological settings

Hyojin Kim^{a,*}, Anne-Sophie Høyer^a, Rasmus Jakobsen^b, Lærke Thorling^a, Jens Aamand^b, Pradip Kumar Maurya^c, Anders Vest Christiansen^c, Birgitte Hansen^a

^a Department of Quaternary and Groundwater mapping, Geological Survey of Denmark and Greenland (GEUS), C.F. Møllers Allé 8, Building 1110, DK-8000 Aarhus, C, Denmark

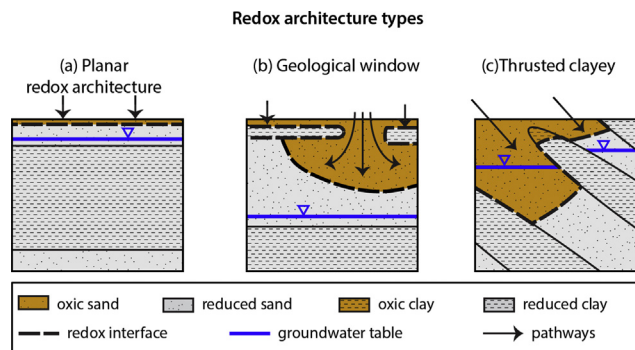
^b Department of Geochemistry, Geological Survey of Denmark and Greenland (GEUS), Øster Voldgade 10, DK-1350 Copenhagen K, Denmark

^c Aarhus University, HydroGeophysics Group, Department of Geoscience, Aarhus, Denmark

HIGHLIGHTS

- Redox architectures were investigated using geophysics and geochemistry data.
- Redox architecture can be complex in glacial deposits with many redox interfaces.
- Three redox architecture types were identified in two glacial-deposit catchments.
- Flows through the deep oxic zone may be an important N pathway to the stream.
- The redox architecture will be key information for the targeted N regulations.

GRAPHICAL ABSTRACT



ARTICLE INFO

Article history:

Received 1 April 2019

Received in revised form 23 July 2019

Accepted 23 July 2019

Available online 26 July 2019

Editor: José Virgílio Cruz

Keywords:

Redox architecture

Hydrogeology

Glacial landscape

Nitrate transport and fate

Targeted N regulations

ABSTRACT

Nitrogen (N) leaching caused by agricultural activities is one of the major threats to the aquatic ecosystems and public health. Moving from the agricultural soils through the subsurface and reemerging to the surface water, N undergoes various biogeochemical reactions along pathways in the subsurface, which occur heterogeneously in space and time. Thus to improve our understanding on the fate and distribution of N in the aquatic environment, detailed knowledge about the subsurface hydrogeological and biogeochemical conditions, especially the redox conditions, are essential. In this study, 3D information of the redox conditions termed the redox architecture was investigated in two Danish catchments with intensive agriculture underlain by glacial deposits. Towed transient electromagnetic (tTEM) resistivity was interpreted which reveals the subsurface geological structures at a few hectare scale. These geophysical data were integrated with sediment and water chemistry for the redox architecture interpretations. The top soils of both catchments are characterized as clay-till, but the tTEM showed that the subsurface hydrogeological structures are distinctively different. We identified three types of redox architectures in the studied catchments: 1) a planar redox architecture with a single redox interface; 2) a geological-window redox architecture with local complexity; and 3) a glaciotectionic-thrusted redox architecture with high complexity. The baseflow N load at the catchment outlets reflect the contributions of N via oxic pathways through the complex redox architectures of the subsurface. We conclude that in some landscapes, the redox architecture cannot be simplified as a single interface that roughly follows the terrain; hence, thorough investigations of the structural heterogeneity of the local redox architectures will be necessary to improve simulations of N evolution along pathways and quantifications of N attenuation under various mitigation scenarios.

© 2019 Elsevier B.V. All rights reserved.

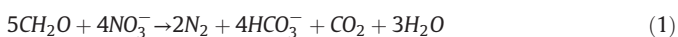
* Corresponding author.

E-mail addresses: hyojin820.kim@gmail.com, hk@geus.dk (H. Kim).

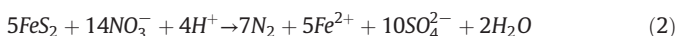
1. Introduction

Extensive efforts have been carried out to reduce the impact of agricultural nitrogen (N) to the aquatic environments during the last four decades at the national level in Denmark (Dalgaard et al., 2014; Hansen et al., 2017). However, to meet the requirements of the European Union's Water Directives, there is still a need for improving the effectiveness of the N regulations that will further reduce the N load to the environment without compromising the agricultural productivity (Danish Nature Agency, 2016). These challenges mimic the situation in many countries e.g. in Europe, the U.S., and New Zealand and promote active research (e.g., Doody et al., 2012; Hashemi et al., 2018; Jha et al., 2010; Rivas et al., 2017; Stenger et al., 2018; Teshager et al., 2017; Thomas et al., 2016; Uthes et al., 2010). To achieve the goal of both N load reduction and high crop production, the N regulations need to scale down to the local field level to be cost effective (Commission on Nature and Agriculture, 2013). Such regulations, which are often named targeted regulations, will be developed for delineated vulnerable or robust areas based on detailed knowledge on the subsurface environment such as soil type, geology, hydrogeology, and biogeochemistry.

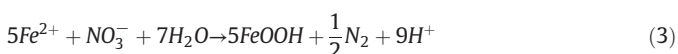
N concentration in water depend on the redox conditions, which can be described in three sequential zones: 1) an oxic zone; 2) a nitrate-reducing zone; and 3) a reduced zone. In the oxic zone, when oxygen is present, N removal is limited or absent. Under nitrate reducing conditions, oxygen has been depleted and microorganisms start to use nitrate as an electron acceptor often coupled with fresh organic carbon as an electron donor (i.e., denitrification; Appelo and Postma, 2010):



when organic carbon is not bioavailable, nitrate is reduced through pyrite oxidation and, to a lesser extent, through oxidation of structural Fe (II) of minerals (e.g., Appelo and Postma, 2010; Böhlke et al., 2002; Ernstsen, 1996; Postma et al., 1991; Tesoriero et al., 2000):



and



In the reduced zone, e.g., Fe/sulfate-reducing or methanogenic zones, nitrate will not be found. These redox reactions increase the product concentrations and decrease the reactant concentrations. Therefore, the redox conditions and dominant redox reactions can be inferred from the concentrations of these redox sensitive elements in water (e.g., Close et al., 2016; Hansen et al., 2016; McMahon and Chapelle, 2008; Rivas et al., 2017; Wilson et al., 2018). The redox conditions can also be inferred from geochemical analysis on solid materials such as soil, sediments and rocks (e.g., Best et al., 2015; Hansen et al., 2008; Postma et al., 1991) and their colors (e.g., Hansen et al., 2016, 2008; Hansen and Thorling, 2008).

In principal, the subsurface redox conditions develop through the mass balance between the cumulative influx of oxidants through the land surface and the amount of reductants in the subsurface. Therefore, the development in redox condition is often shown as a vertical profile with a transition from oxic to progressively reduced conditions with increasing depth. However, reality may be more complicated especially under unconsolidated heterogeneous deposits such as glacial deposits, alluvial sediments, or volcanic deposits (e.g., Best et al., 2015; Böhlke et al., 2002; Carlyle and Hill, 2001; Hansen and Thorling, 2008; Janot et al., 2016; Richards et al., 2017). Under such systems, the types and distributions of the reductants can be spatially heterogeneous (e.g., Best et al., 2015; Janot et al., 2016; Rodvang and Simpkins, 2001; Stenger et al., 2018). In addition, the oxidant pathways may follow a

complicated network, leading to what we have termed a redox architecture. Therefore, the upscaling of the point measurements of the redox conditions to larger scales (e.g., catchment level) under these types of geology is challenging.

Recently, various geophysical techniques have been employed to improve mapping of the subsurface hydrogeology (e.g., Chandra et al., 2019; Comas et al., 2018; Maurya et al., 2018; St. Clair et al., 2015). Depending on the method, the geophysical techniques measure one or more physical properties of the underlying materials. From the geophysical models, hydrological properties can be interpreted. However, these methods are either limited to 2-D transects (e.g., Comas et al., 2018; St. Clair et al., 2015) or, if available in 3D, the spatial resolution is too coarse (e.g., Hansen et al., 2014; Hansen et al., 2016; Refsgaard et al., 2014); therefore, they cannot resolve the complexity at the scale of an agricultural field.

In this study, we attempt to characterize the redox architecture at hectare scale at a catchment level in the context of the targeted N regulations. A newly develop ground-based geophysical instrument referred to as a towed transient electromagnetic method (tTEM) is capable of mapping the near-surface (<50 m depth) at a high resolution (Auken et al., 2018). In this study, the modelled tTEM data are used in combination with geochemical data in two Danish catchments. The primary objective of the study is to characterize the subsurface redox architecture by synthesizing the tTEM model with geological and geochemical information. Then, the role of redox architectures in controlling stream N concentrations and N fluxes at the catchment scale is analyzed. The stream chemistry represents a final output of the interplay between hydrological and biogeochemical processes within the catchment. Therefore, the second objective of this study is to investigate the importance of a better understanding of the redox architecture by analyzing the stream chemistry.

2. Background information

2.1. Site descriptions

This study was conducted in two headwater catchments – Javngyde and Sillerup – Jutland, Denmark. Both catchments are situated in glacial landscapes formed during the Weichselian glaciation (Houmark-Nielsen, 2004; Smed, 1981). Glacial settings are highly heterogeneous at both small- and large- scales. At the small scale, the heterogeneity is, for instance, represented by the clay-till, which is an unsorted glacial sediment consisting of a mixture of clayey and more coarse-grained materials at varying ratios. The large-scale landscape elements are shaped by erosion (e.g., tunnel valleys; Jørgensen and Sandersen, 2006), deposition (e.g., meltwater plains, end moraines), and/or deformation (e.g., thrusts, faults; Høyer et al., 2013; Pedersen, 2005, 1996) processes during advance and retreat of ice-sheets.

Javngyde (catchment area 10.5 km²) is a headwater catchment in the Gudenå watershed. The topography of Javngyde is relatively steep ranging from 90 to 110 m above sea level in the western part of the catchment to 20–30 m above sea level in the valley near the outlet of the catchment (Fig. 1a). The surface soil of the entire catchment is clay-till, except a small area around the valley dominated by freshwater and meltwater sandy deposits (Fig. 1b; Pedersen et al., 2011). In Javngyde, 98% of the area is used by agriculture (82% non-irrigated arable land and 16% for agriculture with significant natural vegetation; Fig. 1c). Javngyde is artificially drained.

Sillerup (30.5 km²) is a headwater catchment of the Sillerup stream. The surface topography is relatively smooth (Fig. 1d). Like Javngyde, the surface soil is categorized as clay-till with small patches of meltwater sand deposits or sandy till in the lower part of the catchment (Fig. 1e; Pedersen et al., 2011). Sillerup is also drained. Sillerup is mainly covered by non-irrigated arable land (74%), forest (13.4%), agricultural land with natural vegetation (5%), and urban areas (0.1%; Fig. 1f).

Javngyde

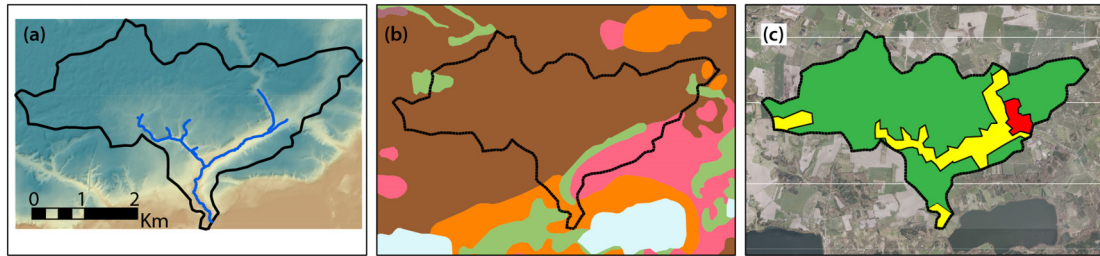


Fig. 1. Site characteristics of the study sites. Maps of surface topography, surface soil type, and land use of Javngyde (1a, 1b, and 1c, respectively) and Sillerup (1d, 1e, and 1f, respectively).

2.2. Nitrate in groundwater

In Denmark, groundwater is the sole source of drinking water. N contamination has been one of the major public health concerns related to drinking water quality (e.g., Schullehner et al., 2018; Schullehner and Hansen, 2014). Groundwater, therefore, has been monitored regularly in the last 30 years. The basic borehole information and groundwater monitoring data are registered on the National Borehole Database (JUPITER) managed by Geological Survey of Denmark and Greenland (Geological Survey of Denmark and Greenland (GEUS), 2018).

The JUPITER data from both sites show that the groundwater table and groundwater nitrate concentrations vary spatially within the catchment. In general, Javngyde has deeper groundwater table and higher nitrate concentrations in groundwater than Sillerup. In Javngyde, the depths to the groundwater table differ significantly between the western (40–60 m) and eastern (10–20 m) parts of the catchment (Fig. 2b). There are 3 monitoring wells, 52 private drinking water abstraction wells, and 3 public drinking water abstraction wells (Fig. 2c) with nitrate measurements. The sampling depth information of most of the private and some public wells is not available. The nitrate concentrations of these private wells were highest (up to 150 mg L⁻¹) especially around the stream (Fig. 2c). Except at two wells, the nitrate concentrations were <1 mg L⁻¹ in groundwater with sampling depth information (Fig. 3a).

In Sillerup, the depths to the groundwater table were shallower than in Javngyde, particularly in the lowland of the catchment (<15 m; Fig. 2e). There are 4 monitoring wells, 30 private drinking water abstraction wells, and 2 public drinking water abstraction wells with

nitrate data (Fig. 2f). The Sillerup groundwater shows nitrate concentrations lower than the groundwater standard level (50 mg L⁻¹) throughout the catchment (Fig. 2f). The average nitrate concentrations of monitoring wells, private drinking water abstraction wells, and public drinking water abstraction wells were 0.5 (min.-max.: not detected – 1.9) mg L⁻¹, 3.5 (not detected – 33) mg L⁻¹, and 1.6 (0.6–2.4) mg L⁻¹, respectively.

3. Method

3.1. tTEM measurements

The resistivity of the shallow subsurface were measured using the tTEM instrument (Auken et al., 2018) in Javngyde and Sillerup from August to November in 2017. The tTEM system is consisted of a set of a transmitter frame and a receiver coil at a 9 m offset that is towed by an all-terrain vehicle (Auken et al., 2018). The spacing between tTEM survey lines was 20–30 m and the vertical resolution of the tTEM data was 2–5 m increasing with depth. The depth of the investigation was 40–60 m, depending on the sediment types. Detailed descriptions of the instrumentation, the field survey methods, and the data processing protocols can be found in Auken et al. (2018).

In Javngyde, tTEM surveys were carried out at 61% of the arable land (5 km²; Fig. 2a). The rest of the arable land was not mapped either because of crop vulnerability or access restriction by the field owners. In Sillerup, about 73% (16 km²) of the arable land was surveyed (Fig. 2d). The rest of the arable land (27%; 5.7 km²) was not mapped mainly because of access restrictions.

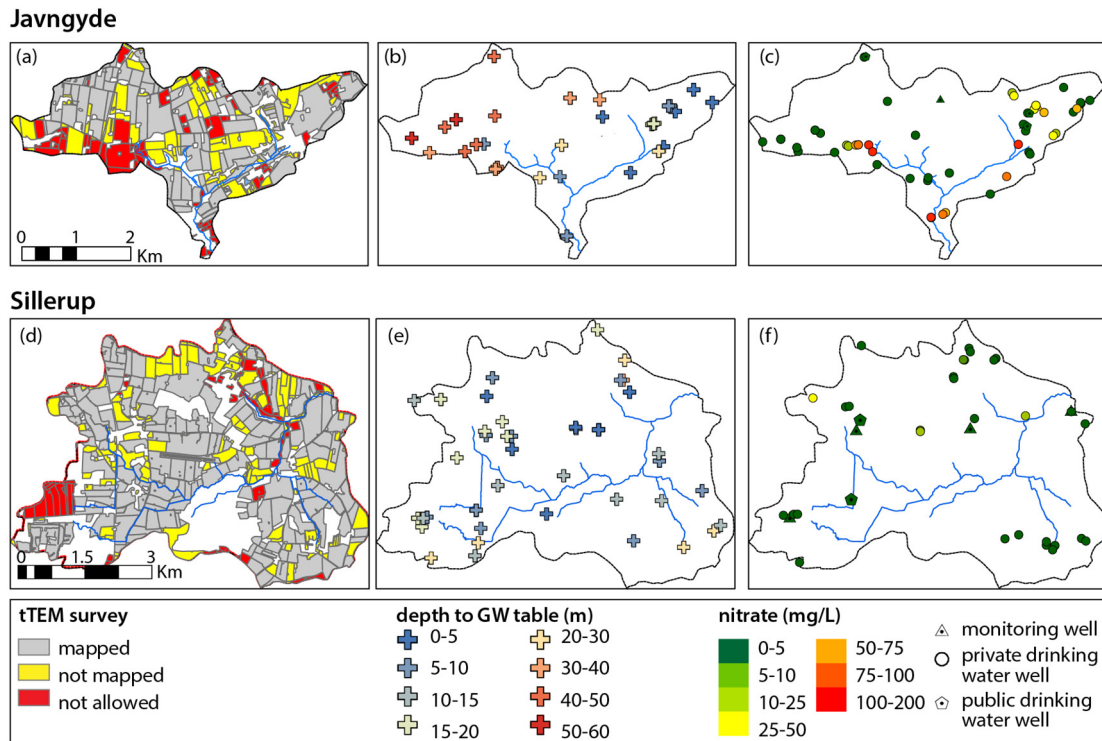


Fig. 2. Maps of the tTEM survey coverage, depth to the groundwater table, and nitrate concentrations (mg L^{-1}) in groundwater in Javngyde (2a, 2b, and 2c, respectively) and Sillerup (2d, 2e, and 2f, respectively).

3.2. Geological interpretation of the subsurface structure

The tTEM data were processed and inverted into geophysical models as described in Auken et al. (2018). The models were then geologically interpreted together with existing data using GeoScene3D (I-GIS, 2018). The existing data include 1) the lithology descriptions of boreholes registered on JUPITER; 2) topographic maps; 3) surface soil maps (Jakobsen et al., 2011; Pedersen et al., 2011); and 4) previous research, including landscape analyses (Smed, 1981) and mapping of buried valleys (Sandersen and Jørgensen, 2016).

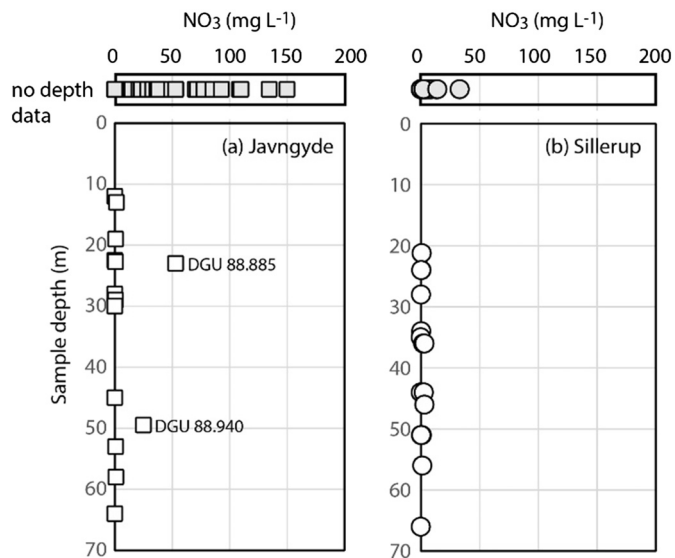


Fig. 3. Nitrate concentrations against the sampling depth in Javngyde (3a) and Sillerup (3b). For the most private water wells, information about the sampling depths is not registered on JUPITER and these data are shown in the upper panels of each figure.

3.3. Subsurface redox condition

Redox conditions of the subsurface of the study sites were inferred from the sediment colors of the boreholes registered on JUPITER. The sediment colors under the Danish conditions are usually a good indicator for the redox conditions and have been used to estimate the depth to the redox interface (Ernstsen and Platen, 2014; Hansen et al., 2016; Hansen and Thorling, 2008). Here, the redox conditions were identified only as oxic and reduced because it is difficult to define representative colors for the nitrate-reducing zone. Red, yellow, brown colors and combinations of these colors are clear indicators of oxic condition. Gray, blue, green, and olive are typical reduced condition colors. Black and dark brown colors indicate a high content of organic matter; therefore, sediments with these colors may likely be reduced.

The number of redox condition shifts (i.e., redox interfaces) were counted. The very top surface of the soil, in contact with the atmosphere, was assumed to be oxic and minor variations in the redox conditions (<1 m thick) were not counted. The depth to the first interface of an oxic to reduced shift was also estimated.

3.4. Groundwater redox state

The redox states of the groundwater were evaluated based on the redox sensitive element concentrations: dissolved oxygen (DO), nitrate, iron, and sulfate. Only a limited number of data was available for each catchment, so we included boreholes in close vicinity of the catchment boundary. For some drinking water wells, all water samples were collected after the drinking water treatments (i.e., aeration and sand filtration). Therefore, these data are not included in the redox evaluation.

Under Danish conditions, the redox states of groundwater is defined as follows (Hansen et al., 2011; Table 1): 1) high DO ($\geq 1 \text{ mg L}^{-1}$) and nitrate ($> 1 \text{ mg L}^{-1}$) as an oxic condition; 2) $< 1 \text{ mg L}^{-1}$ of DO and $> 1 \text{ mg L}^{-1}$ of nitrate as a nitrate-reducing condition; 3) high iron ($\geq 0.2 \text{ mg L}^{-1}$) and sulfate ($\geq 20 \text{ mg L}^{-1}$) but low nitrate ($\leq 1 \text{ mg L}^{-1}$)

Table 1
Criteria for groundwater redox state interpretations.

	Oxic	Nitrate-reducing	Fe/sulfate-reducing	Sulfate-reduced	Mixed water
DO*	≥1 mg L ⁻¹	≤1 mg L ⁻¹	-	-	-
NO ₃ ⁻	>1 mg L ⁻¹	>1 mg L ⁻¹	≤1 mg L ⁻¹	≤1 mg L ⁻¹	>1 mg L ⁻¹
Fe ²⁺	-	-	≥0.2 mg L ⁻¹	≥0.2 mg L ⁻¹	≥0.2 mg L ⁻¹
SO ₄ ²⁻	-	-	≥20 mg L ⁻¹	<20 mg L ⁻¹	-

* Dissolved oxygen.

as an Fe/sulfate-reducing condition; and 4) low sulfate (<20 mg L⁻¹) with high Fe (≥0.2 mg L⁻¹) and low nitrate (≤1 mg L⁻¹) as a sulfate-reduced condition. When groundwater shows simultaneously high iron and high nitrate, it is interpreted as a mixture of groundwater with different redox states.

3.5. Stream nitrogen and annual nitrogen yields in Javngyde and Sillerup

Discharge and total N (hereafter N refers to total N) concentrations of the streams in Javngyde and Sillerup were obtained from the Environmental Protection Agency of Denmark (EPA). The Danish EPA measures several N species including nitrate, nitrite, ammonium, and ammonia as well. However, these are at trace levels except nitrate and the data are available for only limited periods. The concentrations of total nitrogen nearly equals to those of nitrate; therefore, this study used the total N

data only. In Javngyde, the daily discharge and N concentrations in stream water have been monitored (1–2 times a month) since 1989 at the catchment outlet. In Sillerup, the stream discharge has been monitored daily at the catchment outlet for the last 20 years (since 1986) and N had been monitored at 2–3 times a month from December 1992–January 2007.

Volume-weighted annual averages of the measured N concentrations of the Javngyde and Sillerup streams were calculated for a calendar year over the monitoring period and then trends of the annual averages were analyzed using Excel's data analysis package (Regression). The annual yield of N (N_T ; kg N ha⁻¹ y⁻¹) was then estimated by dividing the sum of the daily N fluxes for a calendar year by the catchment area (A ; ha; Eq. (4)):

$$N_T = \left(\sum [N_i] q_i \right) / A \tag{4}$$

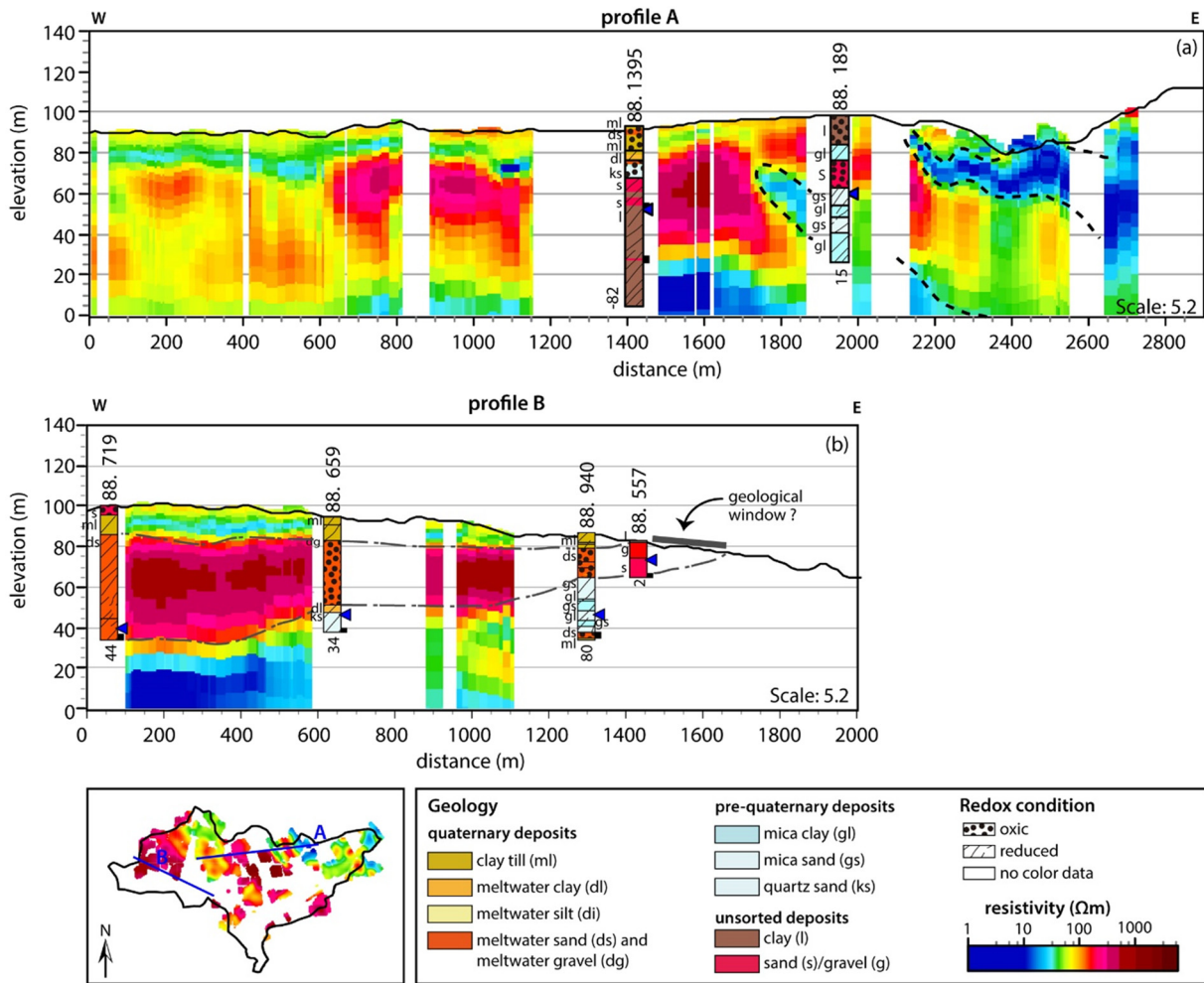


Fig. 4. Resistivity and borehole lithology descriptions in Javngyde. The index map shows the resistivity of elevation at 60 m and locations of profile A and B. The buffer boundaries of the tTEM sounding and JUPITER data were 50 m and 100 m, respectively. The numbers at the top and bottom of the boreholes represent the borehole ID number (DGU number) registered on JUPITER and the distance between profile line and borehole, respectively. The blue triangles and black box next to the boreholes show the groundwater table depth and the screened interval, respectively. Note the vertical exaggeration is x5.2. (For interpretation of the references to colour in this figure legend, the reader is referred to the web version of this article.)

where $[N_i]$ and q_i , are the N concentration in stream (mg L^{-1}) and the total volume of discharge (L) of the i^{th} day of a year. Unmeasured $[N_i]$ was estimated from a power law function of the concentration-discharge (C-Q) relationship for each year (Godsey et al., 2009; Kim et al., 2017):

$$[N_i] = aq_i^b \tag{5}$$

where a and b are coefficients estimated from the C-Q relationships.

The annual N yields via baseflow were calculated as well. The baseflow of Javngyde and Sillerup was estimated using a Web-based Hydrograph Analysis Tool (WHAT; Lim et al., 2005). In our study, the recursive digital filter for perennial streams with porous aquifers was used (filter parameter (α) 0.98; maximum baseflow index (BFI_{max}) = 0.80). The recursive digital filter method automatically filters out a high-frequency signal, which is interpreted as a fast-flowing component i.e., event waters, from a low-frequency signal, which is interpreted as a slow-flowing component i.e., groundwater (Eckhardt, 2005; Lim et al., 2005). Although tile-drain flow is often considered as a fast-flowing component, it also significantly increases the baseflow fraction (Blann et al., 2009; Halford and Mayer, 2000; Schilling and Libra, 2003). To estimate the groundwater discharge components in the baseflow, further research may be required such as hydrological modelling or water chemistry studies using water isotope or conservative tracers. Our study sites are artificially drained and the baseflow in this study, thus, refers to all the slow-flowing components via both tile-drains and groundwater discharge.

The N concentrations at baseflow were volume-weighted averages of the N concentrations of the three lowest discharge points in a single year. Trends of the annual baseflow N were analyzed using Excel as

well. Assuming this N concentration is representative of the baseflow N of each year, the annual yields of N via baseflow were calculated as follows (Eq. (6)):

$$N_B = Q_j B_j [N_b]_{j/A} \tag{6}$$

where Q_j , B_j , and $[N_b]_j$ are the volume of the total annual discharge (L), the fraction of baseflow calculated using WHAT, and the baseflow N concentrations (mg L^{-1}) for the year j . The N yield via non-baseflow was the difference between N_T and N_B . The N yields between two study sites were compared using Excel's data analysis package (t -Test).

4. Results

4.1. Geological interpretations of Javngyde and Sillerup tTEM models

The tTEM models of Javngyde showed that the eastern part of the catchment has a highly complicated structure while the western part shows relatively homogeneous features (Fig. 4). For example, as shown in Fig. 4a, dipping low-resistivity structures are seen in the eastern part of the profile (marked with dotted lines at around profile distance 1700–2700 m). In the horizontal cross-section at elevation 60 m (index map of Fig. 4), these low-resistivity structures show a lobate shape, which is consistent with the shape of glaciotectonic thrust structures. Consistent with this, multiple boreholes in the area describe pre-Quaternary deposits overlying Quaternary deposits (e.g. Fig. 4a, DGU 88.189 and Fig. 4b, DGU 88.940). Such clayey thrust structures are observed throughout the eastern part of the catchment. Although signs of glaciotectonic deformation are also observed in the western part of the catchment (Fig. 4b; DGU 88.940), the overall structure of the

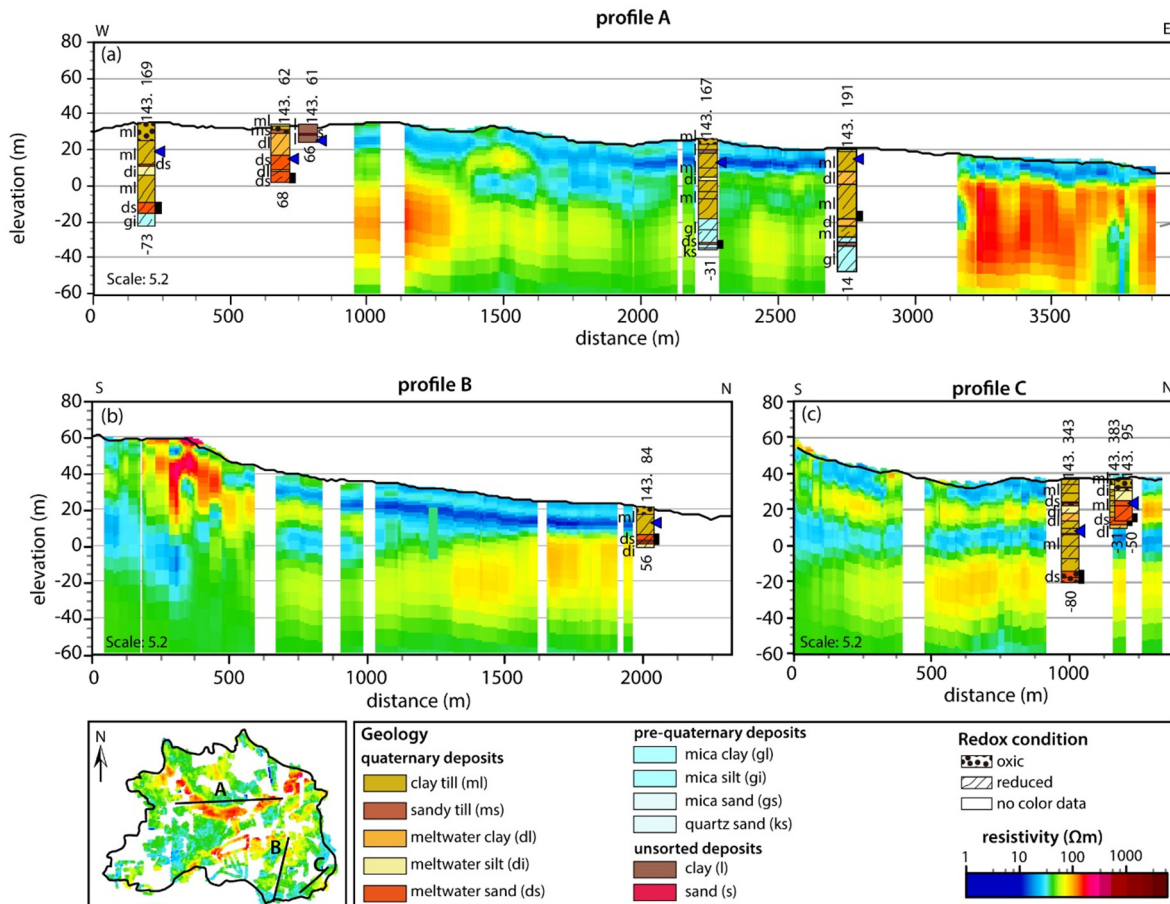


Fig. 5. Resistivity and borehole lithology descriptions in Sillerup. The index map shows the resistivity of elevation at 5 m below the sea level and locations of profile A, B, and C. The buffer boundaries of the tTEM sounding and JUPITER data were 50 m and 100 m, respectively. The elements on this figure are the same as on Fig. 4. Note the vertical exaggeration is 5.2.

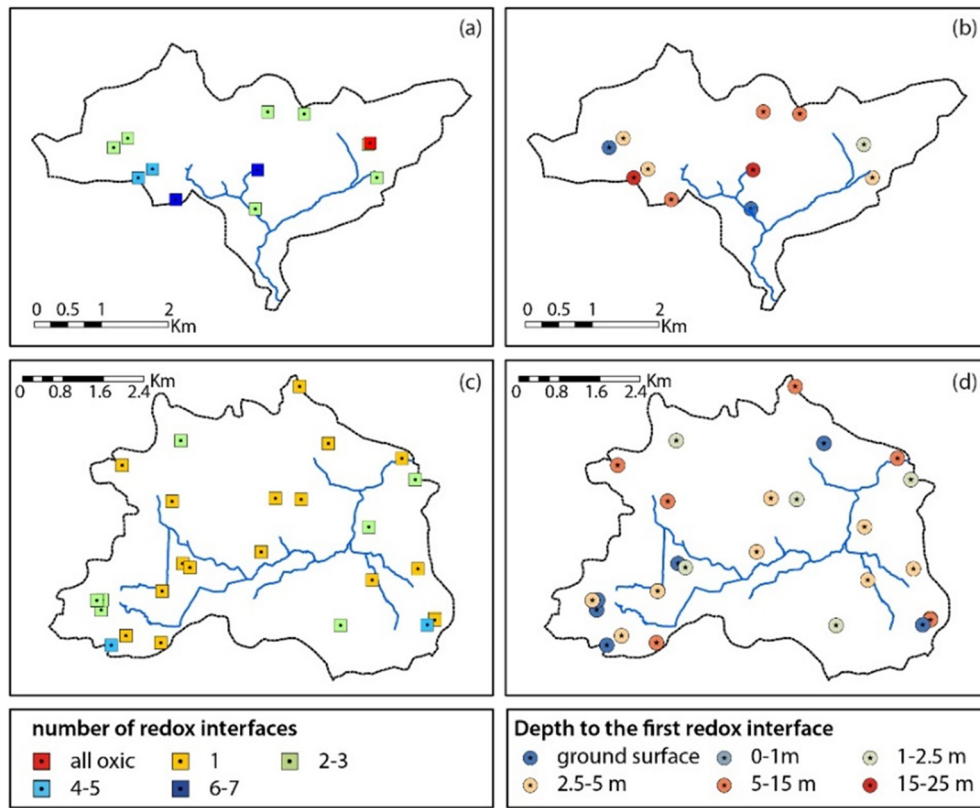


Fig. 6. Depths to the first redox interface (oxic to reduced) and the numbers of redox interfaces of Javngyde (6a and 6b, respectively) and of Sillerup (6c and 6d, respectively). The redox conditions were inferred from sediment colors. The all-oxic well in Javngyde is not shown in Fig. 6b.

subsurface in this area is relatively simple. The western part of the catchment is covered by a low-medium resistivity unit, approximately 10 m thick, which is described as clay-till on the surface soil map (Fig. 1b). This layer is underlain by a thick (~ 40 m) unit of high-resistivity deposits described in the boreholes as meltwater sand and gravel (Fig. 4b). The top clay layer near the stream may be eroded. This may result in direct exposure of the deep sandy zone to the land surface, forming a geological window (Fig. 4b).

Sillerup shows a relatively simple structure across the catchment (Fig. 5). The lowland area in the center of the catchment is covered by a ~ 20 m thick low-medium resistivity layer mainly described as clay-till in the boreholes (Fig. 5a). Below this clay layer, patches of high-resistivity deposits are observed (Fig. 5a, 3120–3875 m). This high-resistivity structure can be followed through the entire area as an elongated structure (index map of Fig. 5) that broadens upwards, which is characteristic for buried valley structures (Jørgensen et al., 2003). The high-resistivity deposits are, therefore, interpreted as coarse-grained infill of a buried valley. At the southeastern boundary of the catchment, a more complex structure is revealed (Fig. 5b, profile distance 0–500 m). According to the landscape analysis, the hill is described as an end-moraine (Smed, 1981). The maximum extent for the ice margin of the East Jutland ice advance is present just west of the study site. Therefore, these end-moraines are probably deposited during a small re-advance or standstill during the overall glacial recession.

4.2. Subsurface sediment redox conditions in Javngyde and Sillerup

The redox conditions in the subsurface of Javngyde and Sillerup also showed contrasting patterns. Javngyde, consistent with the tTEM models and geology, showed complex redox patterns. We found 12 boreholes with continuous records of the sediment colors. One of the boreholes (DGU 88. 917) in the eastern part of the catchment was oxidized throughout the profile of 38 m (Fig. 6a).

In the rest of the boreholes, the redox state shifted at least twice (i.e., oxic → reduced → oxic) and up to six times (Fig. 6a). The first redox interface in Javngyde averaged at 6.7 m below the land surface (mbls), and the shallowest and the deepest interface depths were at the land surface (0 m) and 20.5 mbls, respectively (Fig. 6b). The deep sandy layer in the western part showed the colors indicative of oxic conditions to a depth of 45 mbls (Fig. 4b and Supplementary Fig. 1). The oxic conditions in the eastern part of the catchment follows the sandy zones that are connected to the land surface in between the thrust clayey layers.

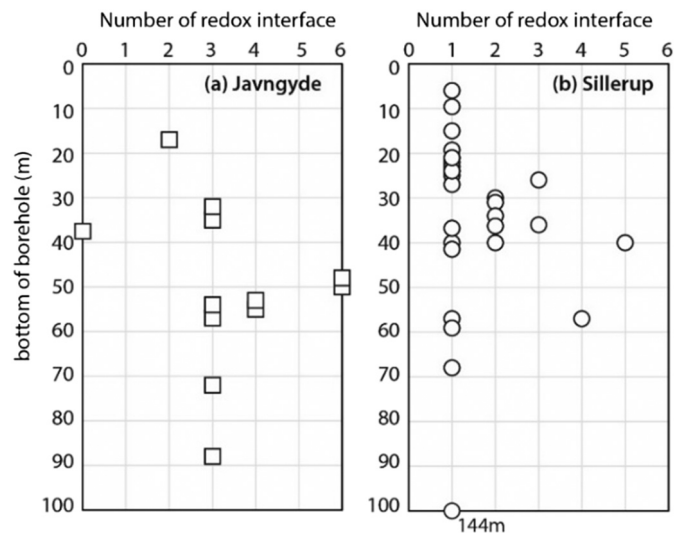


Fig. 7. Number of redox interface against the depth to the bottom of the borehole for the redox condition evaluation of Javngyde (7a) and Sillerup (7b).

In contrast, in Sillerup, in most boreholes, the sediment colors just evolved from oxic to reduced conditions with increasing depth showing a single redox interface (Fig. 6c). In total, 28 boreholes were documented for their sediment colors and 19 of them showed a single redox interface (Fig. 6c). These boreholes were located mainly in the lowland of the catchment near the stream (Fig. 6c), where the thick low-resistivity, clayey layer was revealed by the tTEM models (Fig. 5a). At the remaining 9 boreholes, at least two redox interfaces were identified and these wells were located at the catchment boundary in the higher elevation areas, where the end moraines shape the landscape. The depth to the first interface from oxic to reduced conditions averaged 3.6 mbls and the shallowest and deepest interfaces were found at 0 mbls and 12 mbls, respectively (Fig. 6d).

The redox architecture interpreted from the sediment colors showed that Javngyde has a deeper and more complex structure than Sillerup. One might argue that the contrasting patterns could be due to artifacts related to the differences in the borehole depths. We, therefore, compared the number of redox interfaces and the total depth of each borehole. Indeed, the average depths of the boreholes in Javngyde (49.9 ± 18.6 m) were deeper than that of Sillerup (36.2 ± 26 m). However, as

Fig. 7 shows, the numbers of redox interfaces do not coherently increase nor decrease with increasing total depth of the boreholes. Therefore, we concluded that the difference in the numbers of redox interfaces of two sites reflect actual characteristics.

4.3. Groundwater redox states in Javngyde and Sillerup

Table 2 and Table 3 summarize the concentrations of DO, nitrate, iron, sulfate, and ammonia + ammonium concentrations of the groundwater in Javngyde and Sillerup, respectively. The groundwater chemistry does not show significant temporal variability. In Javngyde, the sampling depths were about 20 m deeper in the western part of the catchment compared to those of the eastern part because of the differences in the depth to the groundwater table (Fig. 2b and Fig. 8). In Javngyde, most groundwater samples displayed no to low oxygen and nitrate while high iron and sulfate, indicating Fe/sulfate-reducing conditions (Table 2). At two locations, which are located near the thrust structures (Fig. 8), indications of mixed redox conditions were observed. A well near the catchment outlet showed moderate levels of DO and nitrate, indicating oxic conditions (Fig. 8).

Table 2
Concentrations of redox sensitive elements and the redox state of the Javngyde groundwater.

DGU number	Intake filter depth (mbls)	Depth to water table (mbls)	Sampling date	O ₂ (mg L ⁻¹)	NO ₃ ⁻ (mg L ⁻¹)	Fe ²⁺ (mg L ⁻¹)	SO ₄ ²⁻ (mg L ⁻¹)	NH ₃ + NH ₄ (mg L ⁻¹)	Redox stage
88. 1395	64–67	40.45	4/24/07	0.17	n.d. ^c	1.4	32	0.085	Fe/SO ₄ -R ^d
			12/6/05	n.d.	n.d.	1.5	40	0.076	
88. 579 ^a (200 m) ^b	60–62	53.5	12/13/04	2.1	n.d.	5.8	83	0.037	Fe/SO ₄ -R
			12/2/98	0.5	n.d.	5.2	74	0.025	
			5/17/93	3.1	n.d.	4.6	72	0.017	
88. 711 ^a (34 m) ^b	55.5–61.5	53.1	7/6/16	0.2	n.d.	0.51	88	0.053	Fe/SO ₄ -R
			11/5/10	0.4	1.1	9.3	81	0.037	
			12/15/09	2.2	n.d.	5.5	85	0.058	
			12/13/04	1	n.d.	5.3	87	0.046	
			12/2/98	n.d.	n.d.	3.6	89	0.044	
			5/17/93	0.4	n.d.	5	80	0.031	
88. 771	58–61	49.7	11/26/13	n.d.	n.d.	1.2	41	0.14	Fe/SO ₄ -R
			10/31/08	0.3	n.d.	1.4	37	0.12	
			11/24/03	n.d.	n.d.	1.6	33	0.1	
			12/2/98	1	n.d.	0.88	36	0.115	
			5/17/93	n.d.	n.d.	0.98	33	0.102	
88. 1105 ^a (67 m) ^b	54–61	46.5	2/3/14	2.8	n.d.	1.8	27	0.2	Fe/SO ₄ -R
			2/18/09	n.d.	n.d.	1.7	26	0.2	
			10/27/04	1	n.d.	1.9	30	0.2	
			11/4/98	1.3	n.d.	1.7	25	0.226	
			5/17/93	1.3	n.d.	1.7	23	0.196	
88. 1121 ^a (100 m) ^b	50–56	46.0	5/7/15	0.3	7.7	0.33	85	0.021	Mixed ^e
			10/9/02	0.9	1.8	1	100	0.008	
			11/5/97	1.2	3.0	0.65	70	0.009	
88. 860 ^a (100 m) ^b	52	14	8/24/92	1.2	n.d.	1.53	59	0.018	Mixed Fe/SO ₄ -R
			5/22/06	3.69	58.0	2	51	0.01	
88. 885	23–29	8	11/10/05	4.94	58.0	1.7	56	0.013	Mixed
			10/11/16	0.2	n.d.	3.9	83	0.05	
88. 917	30–36	18	2/2/12	0.2	n.d.	4.1	78	0.052	Fe/SO ₄ -R
			2/6/07	1.9	n.d.	4.8	76	0.12	
			10/9/02	1.1	n.d.	4.7	88	0.039	
			11/5/197	0.9	n.d.	4	63	0.035	
			8/24/92	1.1	n.d.	7.54	66	0.065	
			2/2/12	0.2	n.d.	7.3	75	0.094	
88. 1002	28–34	19.57	2/6/07	1.3	n.d.	8.2	74	0.19	Fe/SO ₄ -R
			10/9/02	0.9	n.d.	8.4	84	0.067	
			8/24/92	1.1	n.d.	4.13	60	0.038	
			9/7/82	1.8	n.d.	2.51	52	0.02	
			9/14/18	0.4	32	n.d.	64	0.009	
88. 742	25.3–36	11.8	8/7/13	5.4	25	n.d.	59	0.014	Oxic ^f to NO ₃ -R ^g
			3/18/98	4.9	15	n.d.	56	0.026	
			11/21/94	0.5	19	n.d.	66	0.031	

^a Boreholes from outside the catchment boundary.

^b Distance from the catchment boundary.

^c Not detected.

^d Fe/SO₄-reducing conditions.

^e Mixed redox condition.

^f Oxic condition.

^g NO₃-reducing condition.

In Sillerup, the sampling depths of the wells located in the lowland area ranged between 44 and 142 mbls and at least 30 m below the groundwater surface (Table 3 and Fig. 8). The groundwater of these wells showed no nitrate, high iron, and low sulfate concentrations, indicating sulfate-reduced environments (Table 3 and Fig. 8). In contrast, the groundwater from the southwest boundary showed high DO and nitrate concentrations (Table 3 and Fig. 8), indicating oxic conditions.

4.4. Nitrogen in Javngyde and Sillerup streams

In general, the N concentrations in the stream outlet were higher in Javngyde than in Sillerup throughout the observation period. The volume-weighted annual averages of the stream's N concentrations decreased at statistically significant ($p < 0.05$) rates from 1993 to 2006 both in Javngyde (Fig. 9a; slope = $-0.44 \text{ mg L}^{-1} \text{ y}^{-1}$) and in Sillerup (Fig. 9b; slope = $-0.22 \text{ mg L}^{-1} \text{ y}^{-1}$). These decreasing trends may be due to regulations of agricultural N management (Dalgaard et al., 2014).

The inter-annual variability of the annual N yields were strongly influenced by the climate i.e., changes in annual runoff (Fig. 9c and Fig. 9d). In general, the annual N yields decreased over time in the study catchments. For example, Javngyde's annual N yields decreased from $31 \text{ kg N ha}^{-1} \text{ y}^{-1}$ to $21 \text{ kg N ha}^{-1} \text{ y}^{-1}$ and those of Sillerup changed from $38 \text{ kg N ha}^{-1} \text{ y}^{-1}$ to $15 \text{ kg N ha}^{-1} \text{ y}^{-1}$ from 1993 to 2006 (Fig. 9c and Fig. 9d). The annual N yields of these two sites are not significantly different (Table 4; $p \geq 0.05$).

The baseflow N concentrations in the stream outlets were significantly higher in Javngyde than in Sillerup as well. It decreased over time in Javngyde (slope = $-0.10 \text{ mg N L}^{-1} \text{ y}^{-1}$; $p \geq 0.05$; Fig. 9a) while it was relatively invariant in Sillerup (slope = $0.03 \text{ mg N L}^{-1} \text{ y}^{-1}$; $p \geq 0.05$; Fig. 9b) from 1993 to 2006. Both changes are statistically insignificant. The N concentrations at baseflow in Javngyde and Sillerup averaged 3.54 mg L^{-1} (SD 0.87) and 1.42 mg L^{-1} (SD 0.41), respectively. WHAT estimated that in both sites the baseflow contributed on average 66–67% of the annual discharge (Table 4), which is similar to the averages of the baseflow contribution in the similar setting (50–71%; Frederiksen et al., 2018; Zhang et al., 2013). Based on these estimates, about 25% and 15% of the annual N yields of Javngyde and Sillerup, respectively, were attributed to the baseflow (Table 4).

5. Discussion

5.1. The redox architecture of Javngyde and Sillerup

Through the synthesis of the tTEM models, geological interpretations, and redox evaluations from the sediment colors and groundwater chemistry, the redox architecture of our study sites were conceptualized into three types: 1) a planar redox architecture with a single redox interface; 2) a geological-window redox architecture with local complexity; and 3) a glaciectonic-thrusted redox architecture with high complexity (Fig. 10). Fig. 10 shows these three conceptual models and here we simplified lithology to sand and clay in order to represent hydrologically more permeable and less permeable units, respectively. The areas of these redox architecture types for our study sites were identified by estimating the depth to sandy zones using the tTEM models (Fig. 10d and e). In the Danish sediments, resistivity $> 80 \Omega \text{m}$ is interpreted as sand (Thomsen et al., 2004).

In the planar redox architecture, the movement of redox front is primarily vertical (Fig. 10a). Therefore, under this architecture, the redox status progressively evolves from oxic to reduced conditions with increasing depth, resulting in a single redox interface. In this case, the depth to an impermeable boundary may be an important control on the redox architecture. We observed such a type in the lowland of Sillerup where the thick low-resistivity clayey layer (~20 m thick), which forms an effectively impermeable boundary, was documented (Fig. 10e and Fig. 5). The redox state of the groundwater below this low-resistivity layer was sulfate-reduced; therefore, the groundwater is well protected from N contamination.

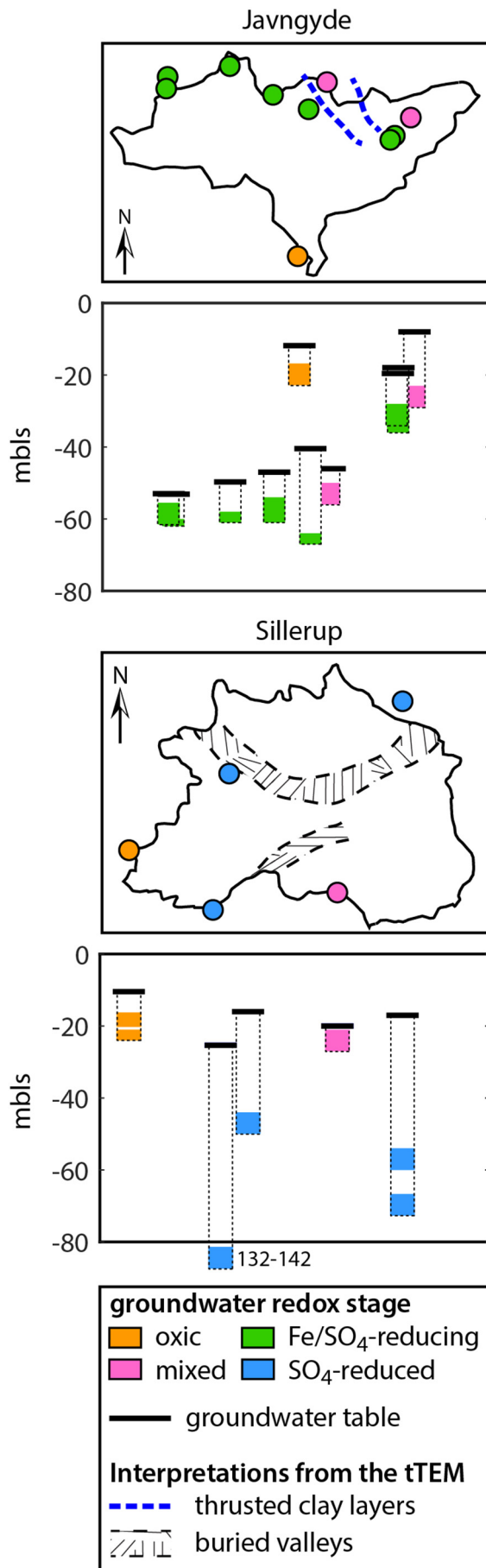
In the geological window redox architecture, oxidants may be delivered into the deeper subsurface through geological windows in the impermeable clayey layer (Fig. 10b). Consequently, oxic conditions will develop mainly around the geological window and the remaining volume of the subsurface may show a relatively simple redox architecture. In this type, the distance to the geological window may be the key parameter in explaining the heterogeneity of the redox architecture. We identified geological windows in the western part of Javngyde (Fig. 10d) and the southern boundary of Sillerup (Fig. 10e). The depths to the sandy zone decrease from north to south (toward the stream) in the western part of Javngyde (Fig. 10d), suggesting a geological window

Table 3
Concentrations of redox sensitive elements and the redox state of the Sillerup groundwater.

DGU Number	Intake filter depth (mbls)	Depth to water table (mbls)	Sampling period	O ₂ (mg L ⁻¹)	NO ₃ ⁻ (mg L ⁻¹)	Fe ²⁺ (mg L ⁻¹)	SO ₄ ²⁻ (mg L ⁻¹)	NH ₃ + NH ₄ (mg L ⁻¹)	Redox stage
142. 975 ^a (56 m) ^b	21–24	10.43	3/6/14	7.4	6.7	0.053	65.7		Oxic
142. 343 ^a (56 m) ^b	17–21	15	5/11/10	1.1	12	n.d.	60	0.021	Oxic
			5/1/07	1.9	12	0.015	60	0.021	
			6/20/01		10	n.d.	47	0.02	
			8/4/97	2.5	8.5	0.06	49	n.d.	
			12/15/94	0.8	8.1	n.d.	53	5.3	
			10/1/90		8.0	0.017	47	0.015	
			8/25/92		n.d.	1.9	17	0.88	SO ₄ -R ¹
143. 126 ^a (430 m) ^b	66.7–77.7	17	12/10/69		3.0	2.8	9.8	0.6	
			9/14/11	0.5	n.d.	2.5	5.8	0.54	SO ₄ -R
			6/12/07	2.3	1.2	2.1	6.6	0.59	
			6/7/00		n.d.	1.5	6.6	0.58	
143. 63 ^a (430 m) ^b	54–60	17	12/11/96	0.8	n.d.	1.8	7.1	0.64	
			8/25/92		n.d.	1.8	6.1	0.56	
			2/1/18	4.3	n.d.	1.8	10.6	0.6	SO ₄ -R
			7/2/15	0.9	n.d.	1.9	9.4	0.52	
			3/8/07	3	n.d.	2.3	6.2	0.55	
			3/18/03	4.3	n.d.	3.6	5.3	0.5	
			8/3/99	0.9	n.d.	2	5.6	0.53	
5/3/95	0.6	n.d.	1.7	6.2	0.53				
143. 235	21–27	20.3	7/3/91		n.d.	1.8	5.9	0.61	
			2/3/76		3	0.69	21	0.2	Mixed
143. 431	132–142	20.4	12/3/07	3.3	0.5	1.5	10	0.44	SO ₄ -R

^a Boreholes from outside the catchment boundary.

^b Distance from the catchment boundary; ¹ SO₄-reduced condition.



in this area. Around this area, groundwater of the private wells shows high nitrate (Fig. 2c), which is consistent with oxic conditions near the geological window and higher vulnerability of groundwater. In Sillerup, the end-moraines in the southern boundary act as the geological window.

In the glacio-tectonically thrustured redox architecture, oxidants predominantly move through the sandy zones between the thrustured clayey layers (Fig. 10c). Consequently, the redox architecture will be complicated and spatially heterogeneous. Under these conditions, high-resolution information of the hydrogeological structure will be critical to predict the redox architecture. We found such a type in the eastern part of Javngyde (Fig. 10d). In this area, the depths to the sandy layer vary significantly within a short distance (Fig. 10d), consistently indicating high spatial heterogeneity. Furthermore, the redox state of the groundwater in this area was mixed to Fe/sulfate-reducing conditions, implying heterogeneity of the redox conditions as well (Fig. 8).

5.2. Redox architecture and the catchment N yields

The redox architectures of Javngyde and Sillerup provide near-direct views of nitrate pathways in the subsurface, which are essential for evaluating the vulnerability of the groundwater to nitrate contamination and to identify primary pathways of nitrate yields in each catchment. In Javngyde, the oxic zones have been developed even in the deep subsurface and some groundwater shows the mixed redox signatures of oxic to Fe/sulfate-reducing conditions at depth (Fig. 8). Consistently, a moderate level of nitrate was also observed in groundwater at 50 mbls (DGU 88. 940; Fig. 3a), which was sampled at the second oxic layer about 10 m below the groundwater table (Fig. 4b). Javngyde's complicated redox architecture indicates that some groundwater in Javngyde may route only through the oxic zones to the stream; consequently, N emerges back to the stream. While in Sillerup, the redox architecture is planar with a single redox interface at shallow depths (average 3.6 mbls). Below the interface, groundwater is in sulfate-reduced conditions (Fig. 8). Therefore, N passing through Sillerup's deeper pathways may be completely reduced in the subsurface and the stream therefore shows low N concentrations.

The stream chemistry, particularly the baseflow chemistry, confirms these explanations. During the baseflow, when groundwater and slow-flowing drain flow were the predominant sources of the stream discharge, the stream N concentrations were much higher in Javngyde than in Sillerup (Fig. 9). This baseflow is also a quantitatively important pathway for the overall N budget of Javngyde. The baseflow's contribution to the annual N yield was higher in Javngyde (average 24%) compared to that in Sillerup (average 15%; Table 4). The differences in the background N concentrations in the streams (i.e., baseflow N concentrations) may result in generally higher N concentrations in Javngyde than in Sillerup.

Based on the stream observations and the redox architecture, we further postulated that Javngyde is a transport-controlled system while Sillerup is a reaction-controlled system. In the transport-controlled systems, water moves faster than N can be reduced; therefore, N in the stream will be controlled primarily by hydrological processes such as mixing or dilution (e.g., Lansdown et al., 2015; Ocampo et al., 2006). While in the reaction-controlled systems, N is reduced faster than water transport; consequently, denitrification will be the key control for the N yield (e.g., Lansdown et al., 2015; Ocampo et al., 2006). Altogether, we propose that the high-resolution information on the subsurface hydrogeology and redox architecture improve our conceptual understanding on the transport pathways and evolution of N in the subsurface as well as on the underlying processes for the N dynamics at the catchment level.

Fig. 8. Groundwater redox state in Javngyde and Sillerup. The locations of the boreholes are shown in the upper panel and the depths of the groundwater samples are shown in the bottom panel for each study site.

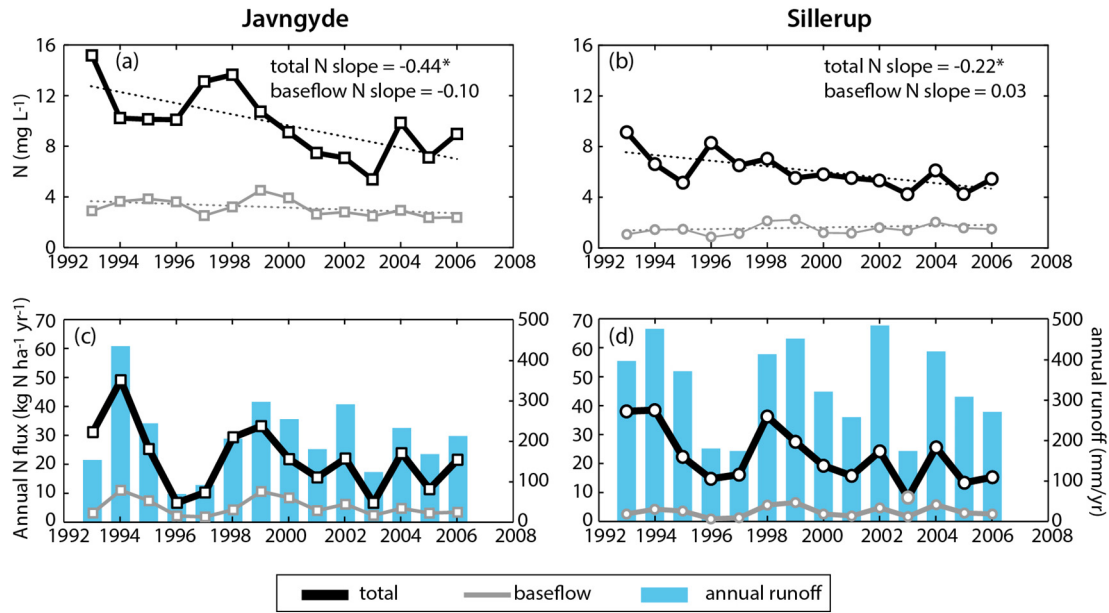


Fig. 9. N concentrations in the stream and annual N fluxes of Javngyde and Sillerup. Volume-weighted annual averages of the N concentrations and of baseflow N concentrations in streams are shown in 9a (Javngyde) and in 9b (Sillerup). The statistically significant slopes ($p < 0.05$) are marked with *. The annual N fluxes, the baseflow N fluxes and the annual runoff are shown in 9c (Javngyde) and 9d (Sillerup).

Such information on the pathways and the redox architecture may also contribute to select the best mitigation measures to reduce the N impact on both groundwater and stream water quality (e.g., Rittenburg et al., 2015). The groundwater and stream water respond differently to N leaching from agricultural fields depending on hydrogeological and geochemical redox conditions. Such information is crucial for developing N pollution maps for specific fields that may be applicable for the targeted regulation of N fertilization and management. In Javngyde, for instance, agricultural fields near the geological windows and the sandy zones near the land surface (red areas in Fig. 10d) may need special attention and strict regulations in order to lower the level of N leaching to both groundwater and stream water. The mitigation measures on these fields could be, for example, catch crops, lower nitrogen input, permanent grassland or afforestation (e.g., Dalgaard et al., 2014; Rittenburg et al., 2015). In Sillerup, on the other hand, much attention has to be paid to protect surface waters by lowering N yields during the high-flow regimes. Emission based N mitigation measures such as constructed wetlands or biofilters can be effective in lowering N losses from the catchment (e.g., Rittenburg et al., 2015; Tournebize et al., 2017).

5.3. Integrating the redox architecture in future targeted N regulations

Currently in Denmark, the agricultural N-regulation regarding surface waters, is based on N-emission-demands on the 15 km²-catchment level determined on large scale (500 m grid cells) model simulations (Højberg et al., 2015). These national scale data, however, are too coarse to be efficient if employed in the targeted N regulations, indicating a need for more detailed local information.

In this study, we demonstrated that combining the tTEM models and hydrogeochemical observations is effective for obtaining the high-resolution information of the subsurface redox architecture in local areas. However, to integrate the redox architecture in the targeted N regulations, challenges remain. In this study, the spatial patterns of the redox architecture were well resolved. However, for the targeted N regulations, quantitative evaluations on N reduction is essential. Determining representative reduction rates for the subsections of the redox architecture will be a major challenge. For example, previous research reported that nitrate reduction rates in the saturated zone under the similar settings to ours (i.e., sandy and gravel aquifers in glacial deposits) varied nearly four orders of magnitude (e.g., Puckett and Cowdery, 2002). Both geological controls e.g., types, contents, and reactivity of available electron donors (Stenger et al., 2018) and hydrological controls e.g., varying reactivity along pathways (Kolbe et al., 2019) may play a key role in determining the extent of nitrate reduction. Therefore, these factors may need to be carefully considered in quantitative studies on the reduction capacity and N reduction rates in the future.

Upscaling is another challenge. The data gaps of the tTEM measurement are inevitable and the redox conditions are measured at point or at 1D-profile scales, at best. For instance, in Javngyde, the tTEM survey covered 60% of the agricultural area and the redox information was available at 11 boreholes. Redox architecture of the un-surveyed areas needs to be predicted based on available knowledge. If a planar redox architecture is expected, the redox interface may potentially be estimated through hydrological simulations (e.g., Hansen et al., 2016). However, under complicated redox architectures, this approach may not be applicable. The oxidant pathways will be highly complicated. Furthermore, the complex redox architecture implies heterogeneous

Table 4
Averages of annual runoff and annual N yields of Javngyde and of Sillerup from 1993 to 2006.

	Annual runoff (mm yr ⁻¹)				Annual N yield (kg N ha ⁻¹ yr ⁻¹)			
	Total	Baseflow	Non-baseflow	% Baseflow	Total	Baseflow	Non-baseflow	% Baseflow
Javngyde	211 (25.8) ^a	139 (61.0)	72 (34.3)	66	21.8 (11.6)	5.1 (3.2)	16.7 (9.8)	24.7
Sillerup	332 (110.1)	221 (72.6)	111 (39.4)	67	22.5 (9.7)	3.3 (1.8)	19.2 (8.7)	15.1

^a Standard deviation in parenthesis.

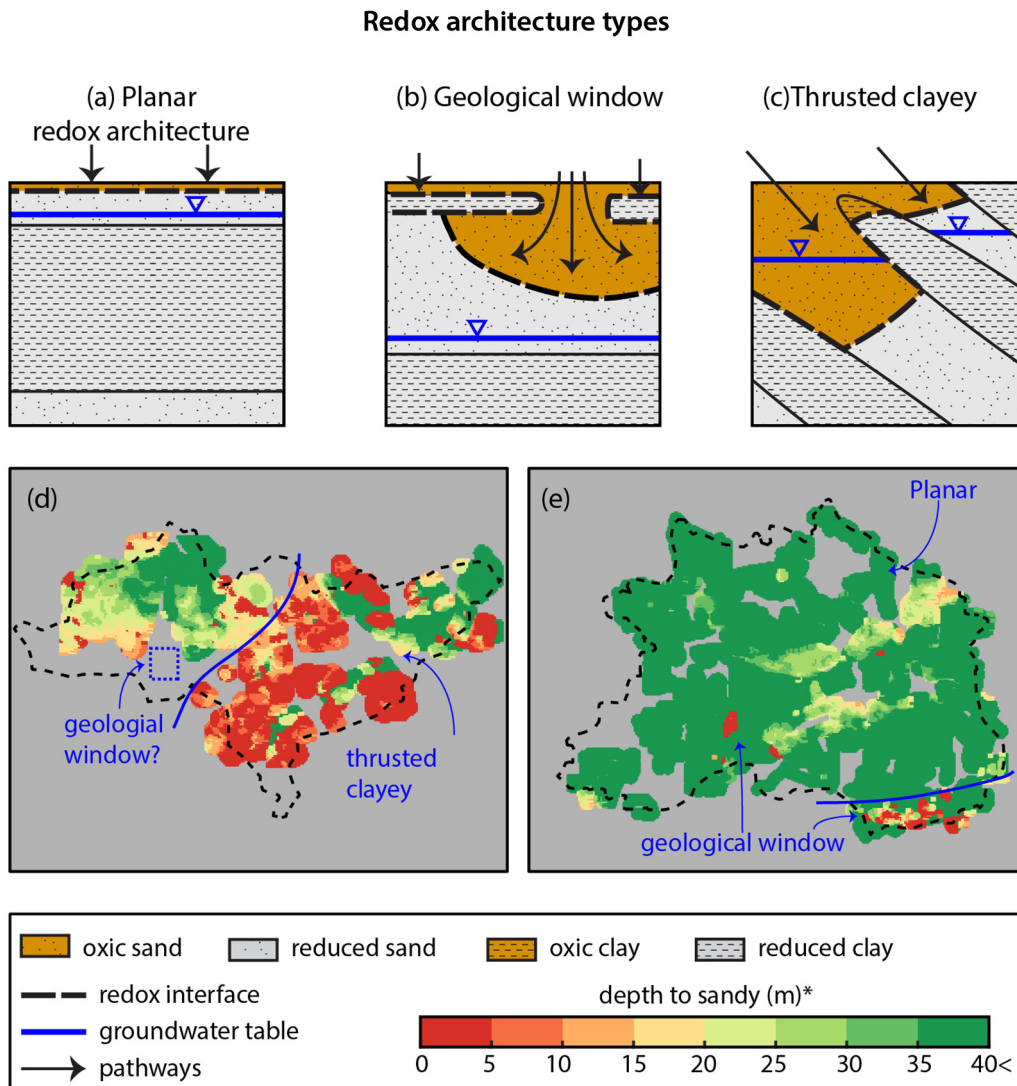


Fig. 10. Conceptual models of three types of redox architecture in Javngyde and Sillerup. *The areas of these redox architecture types in Javngyde (10d) and Sillerup (10e) are delineated by the depth to the sand zone (resistivity $>80 \Omega\text{m}$) estimated from the tTEM data.

reduction capacity of the sediments, which may overwhelm other variables. To address this issue, field data collection needs to be done more strategically and further research is required to explore the applicability of various simulation techniques.

6. Conclusion

In this study, the redox architecture in two Danish catchments of intensive agriculture were investigated by integrating high-resolution, dense tTEM information with geochemical knowledge of water and sediments. In these two sites, three types of redox architectures were identified: 1) a planar redox architecture with a single redox interface; 2) a geological-window redox architecture with local complexity; and 3) a glaciotectionic-thrusted redox architecture with high complexity. Based on the redox architecture and the N concentrations in groundwater and stream water, the dominant pathways of N in the subsurface and N reduction along the pathways were deduced. The redox architecture provided detailed spatial information about the vulnerability of groundwater and surface waters based on the assessment of the zones of nitrate reduction in the subsurface. Here, we conclude that such information is a prerequisite for a successful implementation of the targeted N regulations.

Nearly all the hydrological processes and biogeochemical reactions occur in the subsurface; however, the subsurface is often treated as a black box. In this study, we shed light on the subsurface and explore the importance of the redox architecture for better agricultural N management. Such information may also be important for handling other redox sensitive pollutants such as most geogenic or organic contaminants. We propose that better characterization of the redox architecture will be a fundamental step for the sustainable management and protection of water resources in broader perspectives.

Acknowledgement

We would like to thank three anonymous reviewers for the constructive comments. This project is funded by Innovation Fund Denmark for Open landscape nitrate retention mapping (File Number: 6450-00006B).

Appendix A. Supplementary data

Supplementary data to this article can be found online at <https://doi.org/10.1016/j.scitotenv.2019.133583>.

References

- Appelo, C.A.J., Postma, D., 2010. *Geochemistry, groundwater and pollution*, second edition. Can. J. Microbiol. <https://doi.org/10.1201/9781439833544>.
- Auken, E., Foged, N., Larsen, J.J., Lassen, K.V.T., Maurya, P.K., Dath, S.M., Eiskjær, T.T., 2018. tTEM – a towed TEM-system for detailed 3D imaging of the top 70 meters of the subsurface. *Geophysics* 84, 1–37. <https://doi.org/10.1190/geo2018-0355.1>.
- Best, A., Arnaud, E., Parker, B., Aravena, R., Dunfield, K., 2015. Effects of glacial sediment type and land use on nitrate patterns in groundwater. *Groundw. Monit. Remediat.* 35, 68–81. <https://doi.org/10.1111/gwmr.12100>.
- Blann, K.L., Anderson, J.L., Sands, G.R., Vondracek, B., 2009. Effects of agricultural drainage on aquatic ecosystems: a review. *Crit. Rev. Environ. Sci. Technol.* 39, 909–1001. <https://doi.org/10.1080/10643380801977966>.
- Böhlke, J.K., Wanty, R., Tuttle, M., Delin, G., Landon, M., 2002. Denitrification in the recharge area and discharge area of a transient agricultural nitrate plume in a glacial outwash sand aquifer, Minnesota. *Water Resour. Res.* 38. <https://doi.org/10.1029/2001WR000663> 10-1-10–26.
- Carlyle, G.C., Hill, A.R., 2001. Groundwater phosphate dynamics in a river riparian zone: effects of hydrologic flowpaths, lithology and redox chemistry. *J. Hydrol.* 247, 151–168. [https://doi.org/10.1016/S0022-1694\(01\)00375-4](https://doi.org/10.1016/S0022-1694(01)00375-4).
- Chandra, S., Auken, E., Maurya, P.K., Ahmed, S., Verma, S.K., 2019. Large scale mapping of fractures and groundwater pathways in crystalline hardrock by AEM. *Sci. Rep.* 9, 1–11. <https://doi.org/10.1038/s41598-018-36153-1>.
- Close, M.E., Abraham, P., Humphries, B., Lilburne, L., Cuthill, T., Wilson, S., 2016. Predicting groundwater redox status on a regional scale using linear discriminant analysis. *J. Contam. Hydrol.* 191, 19–32. <https://doi.org/10.1016/j.jconhyd.2016.04.006>.
- Comas, X., Wright, W., Hynek, S.A., Fletcher, R.C., Brantley, S.L., 2018. Understanding fracture distribution and its relation to knickpoint evolution in the Rio Icacos watershed (Luquillo critical zone observatory, Puerto Rico) using landscape-scale hydrogeophysics. *Earth Surf. Process. Landforms*. <https://doi.org/10.1002/esp.4540>.
- Commission on Nature and Agriculture, 2013. *Richer Nature, New Environmental Regulation and New Growth Opportunities for Agriculture* (in Danish).
- Dalgaard, T., Hansen, B., Hasler, B., Hertel, O., Hutchings, N.J., Jacobsen, B.H., Jensen, L.S., Kronvang, B., Olesen, J.E., Schjørring, J.K., Kristensen, I.S., Graversgaard, M., Termansen, M., Vejre, H., 2014. Policies for agricultural nitrogen management-trends, challenges and prospects for improved efficiency in Denmark. *Environ. Res. Lett.* 9. <https://doi.org/10.1088/1748-9326/9/11/115002>.
- Danish Nature Agency, 2016. *Vandområdeplan 2015–2021 for Vandområdedistrikt Jylland og Fyn* (in Danish).
- Doody, D.G., Archbold, M., Foy, R.H., Flynn, R., 2012. Approaches to the implementation of the water framework directive: targeting mitigation measures at critical source areas of diffuse phosphorus in Irish catchments. *J. Environ. Manag.* 93, 225–234. <https://doi.org/10.1016/j.jenvman.2011.09.002>.
- Eckhardt, K., 2005. How to construct recursive digital filters for baseflow separation. *Hydrol. Process.* 19, 507–515. <https://doi.org/10.1002/hyp.5675>.
- Ernstsen, V., 1996. Reduction of nitrate by Fe²⁺ in clay minerals. *Clay Clay Miner.* 44, 599–608. <https://doi.org/10.1346/CCMN.1996.0440503>.
- Ernstsen, V., Platen, F.V., 2014. *Opdatering af det nationale redoxkort fra 2006 – til brug for den Nationale Kvælstofmodel 2015* (in Danish). GEUS rapport 2014/20. Copenhagen).
- Frederiksen, R.R., Christensen, S., Rasmussen, K.R., 2018. Estimating groundwater discharge to a lowland alluvial stream using methods at point-, reach-, and catchment-scale. *J. Hydrol.* 564, 836–845. <https://doi.org/10.1016/j.jhydrol.2018.07.036>.
- Geological Survey of Denmark and Greenland (GEUS), 2018. JUPITER [WWW Document]. URL <https://www.geus.dk/>.
- Godsey, S.E., Kirchner, J.W., Clow, D.W., 2009. Concentration-discharge relationships reflect chemostatic characteristics of US catchments. *Hydrol. Process.* 23, 1844–1864. <https://doi.org/10.1002/hyp.7315>.
- Halford, K.J., Mayer, G.C., 2000. Problems associated with estimating ground water discharge and recharge from stream-discharge records. *Ground Water* 38, 331–342. <https://doi.org/10.1111/j.1745-6584.2000.tb00218.x>.
- Hansen, B., Thorling, L., 2008. *Use of geochemistry in groundwater vulnerability mapping in Denmark*. *Geol. Surv. Denmark Greenl. Bull.* 15, 45–48.
- Hansen, J.R., Ernstsen, V., Refsgaard, J.C., Hansen, S., 2008. Field scale heterogeneity of redox conditions in till-upscaling to a catchment nitrate model. *Hydrogeol. J.* 16, 1251–1266. <https://doi.org/10.1007/s10040-008-0330-1>.
- Hansen, B., Thorling, L., Dalgaard, T., Erlandsen, M., 2011. Trend reversal of nitrate in Danish groundwater – a reflection of agricultural practices and nitrogen surpluses since 1950. *Environ. Sci. Technol.* 45, 228–234. <https://doi.org/10.1021/es102334u>.
- Hansen, A.L., Christensen, B.S.B., Ernstsen, V., He, X., Refsgaard, J.C., 2014. A concept for estimating depth of the redox interface for catchment-scale nitrate modelling in a till area in Denmark. *Hydrogeol. J.* 22, 1639–1655. <https://doi.org/10.1007/s10040-014-1152-y>.
- Hansen, B., Sonnenborg, T.O., Møller, I., Bernth, J.D., Høyer, A.S., Rasmussen, P., Sandersen, P.B.E., Jørgensen, F., 2016. Nitrate vulnerability assessment of aquifers. *Environ. Earth Sci.* 75, 1–15. <https://doi.org/10.1007/s12665-016-5767-2>.
- Hansen, B., Thorling, L., Schullehner, J., Termansen, M., Dalgaard, T., 2017. Groundwater nitrate response to sustainable nitrogen management. *Sci. Rep.* 7, 8566. <https://doi.org/10.1038/s41598-017-07147-2>.
- Hashemi, F., Olesen, J.E., Børgesen, C.D., Tornbjerg, H., Thodsen, H., Dalgaard, T., 2018. Potential benefits of farm scale measures versus landscape measures for reducing nitrate loads in a Danish catchment. *Sci. Total Environ.* 637–638, 318–335. <https://doi.org/10.1016/j.scitotenv.2018.04.390>.
- Højberg, A.L., Windolf, J., Christen Duus, Børgesen, Troldborg, L., Tornbjerg, H., Gitte, Blicher-Mathiesen, Kronvang, B., Thodsen, H., Ernstsen, V., 2015. National kvælstofmodel. Oplandsmodel til belastning og virkemidler: Kortleverancer (in Danish). Copenhagen).
- Houmark-Nielsen, M., 2004. *The Pleistocene of Denmark, a review of stratigraphy and glaciation history*. In: Ehlers, J., Gibbard, P.L. (Eds.), *Quaternary Glaciations - Extent and Chronology: Part 1, Europe*. Elsevier, Amsterdam, pp. 35–46.
- Høyer, A.-S., Jørgensen, F., Piotrowski, J.A., Jakobsen, P.R., 2013. Deeply rooted glaciotectionism in western Denmark: geological composition, structural characteristics and the origin of Varde hill-island. *J. Quat. Sci.* 28, 683–696. <https://doi.org/10.1002/jqs.2667>.
- I-GIS, 2018. *Geoscene3D*.
- Jakobsen, P.R., Hermansen, B., Tougaard, L., 2011. *Danmarks digitale jordarkort 1:25000 Version 3.1*. Danmark og Grønlands Geologiske undersøgelser rapport no. 40.
- Janot, N., Lezama Pacheco, J.S., Pham, D.Q., O'Brien, T.M., Hausladen, D., Noël, V., Lallier, F., Maher, K., Fendorf, S., Williams, K.H., Long, P.E., Bargar, J.R., 2016. Physico-chemical heterogeneity of organic-rich sediments in the rifle aquifer, CO: impact on uranium biogeochemistry. *Environ. Sci. Technol.* 50, 46–53. <https://doi.org/10.1021/acs.est.5b03208>.
- Jha, M.K., Schilling, K.E., Gassman, P.W., Wolter, C.F., 2010. Targeting land-use change for nitrate-nitrogen load reductions in an agricultural watershed. *J. Soil Water Conserv.* 65, 342–352. <https://doi.org/10.2489/jswc.65.6.342>.
- Jørgensen, F., Sandersen, P.B.E., 2006. Buried and open tunnel valleys in Denmark—erosion beneath multiple ice sheets. *Quat. Sci. Rev.* 25, 1339–1363. <https://doi.org/10.1016/j.quascirev.2005.11.006>.
- Jørgensen, F., Sandersen, P.B.E., Auken, E., 2003. Imaging buried quaternary valleys using the transient electromagnetic method. *J. Appl. Geophys.* 53, 199–213. <https://doi.org/10.1016/j.jappgeo.2003.08.016>.
- Kim, H., Dietrich, W.E., Thurnhoffer, B.M., Bishop, J.K.B.B., Fung, I.Y., 2017. Controls on solute concentration-discharge relationships revealed by simultaneous hydrochemistry observations of hillslope runoff and stream flow: the importance of critical zone structure. *Water Resour. Res.* 53, 5375–5377. <https://doi.org/10.1002/2016WR019722>.
- Kolbe, T., de Dreuzy, J.-R., Abbott, B.W., Aquilina, L., Babey, T., Green, C.T., Fleckenstein, J.H., Labasque, T., Laverman, A.M., Marçais, J., Peiffer, S., Thomas, Z., Pinay, G., Babey, T., de Dreuzy, J.-R., Thomas, Z., Marçais, J., Abbott, B.W., Peiffer, S., Aquilina, L., Labasque, T., Kolbe, T., Laverman, A.M., Green, C.T., Pinay, G., 2019. Stratification of reactivity determines nitrate removal in groundwater. *Proc. Natl. Acad. Sci.* 116, 2494–2499. <https://doi.org/10.1073/pnas.1816892116>.
- Lansdown, K., Heppell, C.M., Trimmer, M., Binley, A., Heathwaite, A.L., Byrne, P., Zhang, H., 2015. The interplay between transport and reaction rates as controls on nitrate attenuation in permeable, streambed sediments. *J. Geophys. Res. G Biogeosciences* 120, 1093–1109. <https://doi.org/10.1002/2014JG002874>.
- Lim, K.J., Engel, B.A., Tang, Z., Choi, J., Kim, K.-S., Muthukrishnan, S., Tripathy, D., 2005. Automated web GIS based hydrograph analysis tool, WHAT. *J. Am. Water Resour. Assoc.* 41, 1407–1416. <https://doi.org/10.1111/j.1752-1688.2005.tb03808.x>.
- Maurya, P.K., Balbarini, N., Møller, I., Rønde, V., Christiansen, A.V., Bjerg, P.L., Auken, E., Fiandaca, G., 2018. Subsurface imaging of water electrical conductivity, hydraulic permeability and lithology at contaminated sites by induced polarization. *Geophys. J. Int.* 213, 770–785. <https://doi.org/10.1093/gji/gyy018>.
- McMahon, P.B., Chapelle, F.H., 2008. Redox processes and water quality of selected principal aquifer systems. *Ground Water* 46, 259–271. <https://doi.org/10.1111/j.1745-6584.2007.00385.x>.
- Ocampo, C.J., Oldham, C.E., Sivapalan, M., 2006. Nitrate attenuation in agricultural catchments: shifting balances between transport and reaction. *Water Resour. Res.* 42, 1–16. <https://doi.org/10.1029/2004WR003773>.
- Pedersen, S.A.S., 1996. Progressive glaciotectionic deformation in Weichselian and Paleogene deposits at Feggekliit, northern Denmark. *Bull. Geol. Soc. Denmark* 42, 153–174.
- Pedersen, S.A.S., 2005. Structural analysis of the Rubjerg Knude Glaciotectionic Complex, Vendsyssel, northern Denmark. *Bull. Geol. Soc. Am.* 8 (192 + 192 plates).
- Pedersen, S.A.S., Hermansen, B., Nathan, C., Tougaard, L., 2011. *Digitalt kort over Danmarks jordarter 1:200.000, version 2*: GEUS.
- Postma, D., Boesen, C., Kristiansen, H., Larsen, F., 1991. Nitrate reduction in an unconfined Sandy aquifer - water chemistry, reduction processes, and geochemical modeling. *Water Resour. Res.* 27, 2027–2045.
- Puckett, L.J., Cowdery, T.K., 2002. Transport and fate of nitrate in a glacial outwash aquifer in relation to ground water age, land use practices, and redox processes. *J. Environ. Qual.* 31, 782. <https://doi.org/10.2134/jeq2002.0782>.
- Refsgaard, J.C., Auken, E., Bamberg, C.A., Christensen, B.S.B., Clausen, T., Dalgaard, E., Effersø, F., Ernstsen, V., Gertz, F., Hansen, A.L., He, X., Jacobsen, B.H., Jensen, K.H., Jørgensen, F., Jørgensen, L.F., Koch, J., Nilsson, B., Petersen, C., De Schepper, G., Schamper, C., Sørensen, K.L., Therrien, R., Thirup, C., Viezzoli, A., 2014. Nitrate reduction in geologically heterogeneous catchments - a framework for assessing the scale of predictive capability of hydrological models. *Sci. Total Environ.* 468–469, 1278–1288. <https://doi.org/10.1016/j.scitotenv.2013.07.042>.
- Richards, L.A., Magnone, D., Sovann, C., Kong, C., Uhlemann, S., Kuras, O., van Dongen, B.E., Ballentine, C.J., Poly, D.A., 2017. High resolution profile of inorganic aqueous geochemistry and key redox zones in an arsenic bearing aquifer in Cambodia. *Sci. Total Environ.* 590–591, 540–553. <https://doi.org/10.1016/j.scitotenv.2017.02.217>.
- Rittenburg, R.A., Squires, A.L., Boll, J., Brooks, E.S., Easton, Z.M., Steenhuis, T.S., 2015. Agricultural BMP effectiveness and dominant hydrological flow paths: concepts and a review. *J. Am. Water Resour. Assoc.* 51, 305–329. <https://doi.org/10.1111/1752-1688.12293>.
- Rivas, A., Singh, R., Horne, D., Roygard, J., Matthews, A., Hedley, M.J., 2017. Denitrification potential in the subsurface environment in the Manawatu River catchment, New Zealand: indications from oxidation-reduction conditions, hydrogeological factors, and implications for nutrient management. *J. Environ. Manag.* 197, 476–489. <https://doi.org/10.1016/j.jenvman.2017.04.015>.

- Rodvang, S.J., Simpkins, W.W., 2001. Agricultural contaminants in quaternary aquitards: a review of occurrence and fate in North America. *Hydrogeol. J.* 9, 44–59. <https://doi.org/10.1007/s100400000114>.
- Sandersen, P.B.E., Jørgensen, F., 2016. Kortlægning af begravede dale i Danmark.
- Schilling, K.E., Libra, R.D., 2003. Increased baseflow in Iowa over the second half of the 20th century. *J. Am. Water Resour. Assoc.* 39, 851–860. <https://doi.org/10.1111/j.1752-1688.2003.tb04410.x>.
- Schullehner, J., Hansen, B., 2014. Nitrate exposure from drinking water in Denmark over the last 35 years. *Environ. Res. Lett.* 9, 095001 (9pp). <https://doi.org/10.1088/1748-9326/9/9/095001>.
- Schullehner, J., Hansen, B., Thygesen, M., Pedersen, C.B., Sigsgaard, T., 2018. Nitrate in drinking water and colorectal cancer risk: a nationwide population-based cohort study. *Int. J. Cancer* 143, 73–79. <https://doi.org/10.1002/ijc.31306>.
- Smed, P., 1981. *Landskabskort Midtjylland: Geografforlaget*.
- St. Clair, J., Moon, S., Holbrook, W.S., Perron, J.T., Riebe, C.S., Martel, S.J., Carr, B., Harman, C., Singha, K., Richter, D.D., 2015. Geophysical imaging reveals topographic stress control of bedrock weathering. *Science* (80-) 350, 534–538. <https://doi.org/10.1126/science.aab2210>.
- Stenger, R., Clague, J.C., Morgenstern, U., Clough, T.J., 2018. Vertical stratification of redox conditions, denitrification and recharge in shallow groundwater on a volcanic hill-slope containing relict organic matter. *Sci. Total Environ.* 639, 1205–1219. <https://doi.org/10.1016/j.scitotenv.2018.05.122>.
- Teshager, A.D., Gassman, P.W., Secchi, S., Schoof, J.T., 2017. Simulation of targeted pollutant-mitigation-strategies to reduce nitrate and sediment hotspots in agricultural watershed. *Sci. Total Environ.* 607–608, 1188–1200. <https://doi.org/10.1016/j.scitotenv.2017.07.048>.
- Tesoriero, A.J., Liebscher, H., Cox, S.E., 2000. Mechanism and rate of denitrification in an agricultural watershed: Electron and mass balance along groundwater flow paths. *Water Resour. Res.* 36, 1545–1559. <https://doi.org/10.1029/2000WR900035>.
- Thomas, I.A., Mellander, P.E., Murphy, P.N.C., Fenton, O., Shine, O., Djodjic, F., Dunlop, P., Jordan, P., 2016. A sub-field scale critical source area index for legacy phosphorus management using high resolution data. *Agric. Ecosyst. Environ.* 233, 238–252. <https://doi.org/10.1016/j.agee.2016.09.012>.
- Thomsen, R., Søndergaard, V.H., Sørensen, K.I., 2004. Hydrogeological mapping as a basis for establishing site-specific groundwater protection zones in Denmark. *Hydrogeol. J.* 12, 550–562. <https://doi.org/10.1007/s10040-004-0345-1>.
- Tournebise, J., Chaumont, C., Mander, Ü., 2017. Implications for constructed wetlands to mitigate nitrate and pesticide pollution in agricultural drained watersheds. *Ecol. Eng.* 103, 415–425. <https://doi.org/10.1016/j.ecoleng.2016.02.014>.
- Uthes, S., Matzdorf, B., Müller, K., Kaechele, H., 2010. Spatial targeting of Agri-environmental measures: cost-effectiveness and distributional consequences. *Environ. Manag.* 46, 494–509. <https://doi.org/10.1007/s00267-010-9518-y>.
- Wilson, S.R., Close, M.E., Abraham, P., 2018. Applying linear discriminant analysis to predict groundwater redox conditions conducive to denitrification. *J. Hydrol.* 556, 611–624. <https://doi.org/10.1016/j.jhydrol.2017.11.045>.
- Zhang, Y., Ahiablame, L., Engel, B., Liu, J., 2013. Regression modeling of baseflow and baseflow index for Michigan USA. *Water (Switzerland)* 5, 1797–1815. <https://doi.org/10.3390/w5041797>.